sustainability

MDPI

Article

Characterization of Alkanolamine Blends for Carbon Dioxide Absorption. Corrosion and Regeneration Studies

Alfredo Sánchez-Bautista [1], Ester M. Palmero [1,2], Alberto J. Moya [1], Diego Gómez-Díaz [3] and M. Dolores La Rubia [1,*]

[1] Department of Chemical Environmental and Materials Engineering, Campus Las Lagunillas, Campus Lagunillas, University of Jaén, 23071 Jaen, Spain; abautist@ujaen.es (A.S.-B.); ester.palmero@imdea.org (E.M.P.); ajmoy@ujaen.es (A.J.M.)
[2] Group of Permanent Magnets and Applications, IMDEA Nanoscience, 28049 Madrid, Spain
[3] Department of Chemical Engineering, ETSE, Campus Vida, University of Santiago de Compostela, Rúa Lope Gómez de Marzoa s/n, 15782 Santiago de Compostela, Spain; diego.gomez@usc.es
* Correspondence: mdrubia@ujaen.es

Abstract: There are a lot of research programs focusing on the development of new solvents for carbon dioxide capture. The most important priority should be reducing the energy consumption needed at the regeneration step, but minimizing solvent degradation and its corrosivity is also considered as a priority. In this research, the aqueous blends of 2-amino-2-methyl-1-propanol (AMP: 1 kmol·m^{-3}) and 1-amino-2-propanol (MIPA: 0.1–0.5 kmol·m^{-3}) are characterized in terms of density, viscosity, and surface tension. The carbon dioxide absorption rate and capacity, the regeneration capacity, and the corrosivity of these solvents are also evaluated.

Keywords: carbon dioxide; absorption; 2-amino-2-methyl-1-propanol; 1-amino-2-propanol; electrochemical corrosion; AISI 420; density; viscosity; surface tension; regeneration capacity

Citation: Sánchez-Bautista, A.; Palmero, E.M.; Moya, A.J.; Gómez-Díaz, D.; La Rubia, M.D. Characterization of Alkanolamine Blends for Carbon Dioxide Absorption. Corrosion and Regeneration Studies. *Sustainability* **2021**, *13*, 4011. https://doi.org/10.3390/su13074011

Academic Editor: Adam Smoliński

Received: 8 March 2021
Accepted: 1 April 2021
Published: 3 April 2021

1. Introduction

In recent years, avoiding CO_2 emissions from industries to the atmosphere has been of increasing interest in order to protect the environment [1–3].

On the other hand, many industries, such as synthesis gas for ammonia production, synthetic natural gas, or hydrogen manufacture, need to eliminate acid gases, primarily CO_2 and H_2S, to reduce impurities during the process [4,5]. There are different ways to recover CO_2 from industrial gas streams, but the most widely used and promising process is the absorption using aqueous solutions of alkanolamines. Alkanolamines can be classified into three important groups: primary (e.g., monoethanolamine, MEA), secondary (e.g., diethanolamine, DEA), and tertiary (e.g., methyldiethanolamine MDEA) [6,7].

Many research programs aim at developing new solvents for carbon dioxide capture. The priorities usually are minimizing both energy consumption in the regeneration step and the solvent degradation.

The use of mixtures of alkanolamines has many advantages over the use of simple alkanolamines. Through these mixtures, the benefits of the different types of alkanolamines can be combined and reduce the disadvantages of others [8].

The reaction rates, enthalpies of reaction, and enthalpies of evaporation decrease from primary to tertiary alkanolamines. These enthalpies are directly related to the energy necessary for the regeneration of the solvent.

Gaseous stream treatment plants present corrosion problems which can cause production losses and reduction in equipment life. Corrosion in these plants is due to the presence of acid gases and their high temperature. Different types of corrosion occur in gas treatment plants: general or localized, like pitting, erosion, and stress corrosion [9]. The equipment where most of the severe corrosion problems are found in the reboiler, amine

exchanger, regenerator, condenser, absorber, and amine cooler [6]. Primary and secondary alkanolamines form foams and their degradation products are highly corrosive. This produces solvent losses and increases costs since the use of corrosion-resistant materials is necessary [10].

On the other hand, the absorption capacity of primary to tertiary alkanolamines increases. This implies that higher concentrations are necessary with the consequent environmental and economic effects [11].

If the advantages and disadvantages of the different types of alkanolamines are taken into account, it can be considered that their mixtures could give rise to absorbents with good absorption capacity, fewer corrosion problems, and more profitable from an economic point of view. Among the most studied mixtures are those involving primary or secondary alkanolamines with tertiary alkanolamines with the intention of combining the high absorption capacity of tertiary alkanolamines and the higher absorption speed of primary and secondary alkanolamines [4].

On the other hand, it should be noted that because sterically hindered alkanolamines do not form stable carbamate [12], the amount of bicarbonate and carbonate ions present in the solution is greater than that of carbamate. Therefore, regeneration costs, are lower than for tertiary alkanolamines. For this reason, mixtures of primary and secondary alkanolamines with sterically hindered alkanolamines are being increasingly studied [13–15].

Recently, studies on acid gases recovering by AMP (2-amino-2-methyl-1-propanol) based absorbents have demonstrated that it is a good option because of their high thermal stability, loading capacity, absorption rate, and relatively low regeneration energy [16–20]. The regeneration capacity can be controlled by the deprotonation equilibrium and this behavior can influence reaction kinetics and carbon dioxide absorption rate.

Also, many corrosion studies have been carried out to study the new alkanolamines behavior, like AMP and some of its blends with other amines [21–23]. Most of these studies are focused on carbon steel and only a few of them on high alloyed steels [24,25].

The objective of this work is the characterization of aqueous blends of alkanolamines that are beneficial for the environment and save costs. For this, the sterically hindered AMP and the primary MIPA have been chosen. These mixtures will be analyzed in terms of CO_2 absorption, corrosion, and regeneration capacity.

2. Materials and Methods

2.1. Materials

For the absorption and corrosion experiments, solutions with different compositions were used. Aqueous 2-amino-2-methyl-1-propanol (AMP, 95.0% Panreac) solutions, 1.0 kmol·m^{-3}, and aqueous 1-amino-2-propanol (MIPA, ≥98% purity, Merck) solutions, in the range of 0.1–0.5 kmol·m^{-3}, were prepared using Milli-Q ultrapure water. Then, the different AMP and MIPA solutions were mixed with a concentration of 1:1 (v/v) to obtain the final solutions used in the experiments. CO_2 was N-38, 99.98% SEO.

2.2. Properties Measurements

Experimental data of density corresponding to the different blends employed in the present work have been determined using an Anton Paar DSA 5000 vibrating tube densimeter and sound analyzer.

Kinematic viscosity was determined using a Schott-Geräte AVS 350 Ubbelohde viscosimeter using different capillaries (I, Ic, II, and III), supplied by Schott and using Equation (1).

$$v = K \cdot (t - \theta) \quad (1)$$

where K is the constant of each capillary, t is the efflux time, and θ is a correction parameter. An electronic stopwatch was employed to determine the efflux times. Dynamic viscosity

(η) was calculated using Equation (2) on the basis of experimental values of kinematic viscosity (ν) and density (ρ), previously determined.

$$n = \upsilon \cdot \rho \tag{2}$$

The surface tension of amino-based blends was obtained using a Krüss K-11 tensiometer employing the Wilhelmy plate experimental procedure. The plate used for this type of measurement was a commercial platinum plate supplied by Krüss. This plate was cleaned and flame dried after and before each measurement in order to guarantee the quality of the experimental value. The samples were thermostated before each measurement in a closed vessel.

All measurements were measured at different temperatures (303.15, 313.15, and 323.15 K) in agreement with the other studies included in the present work.

2.3. Absorption Studies in Stirred Cell

Absorption experiments were carried out in a planar stirred tank contactor, using a constant stirring rate of 80 $\pm$ 1 rpm, working on batch with respect to all phases involved in the experimental procedure. The gas-liquid interface was a flat and known interface area (A = 35.26 cm^2). The device employed to develop the absorption experiments is described in previous research work [26].

The carbon dioxide flow densities (N_A) were determined using Equation (3).

$$N_A = \frac{n'}{A} = \frac{PQ'}{RTA} \tag{3}$$

The representation of the carbon dioxide absorbed volume versus time allows us to calculate the value of the volumetric flow (Q') under different experimental conditions using linear fits.

2.4. Absorption Studies in Bubble Column Reactor

Several experiments were carried out using a bubble column with a square geometry (side = 4 cm and height = 65 cm). The chemical solvent volume employed in the contactor was 0.9 L. The gas sparger consisted of a five-hole disk made in Teflon®. In order to evaluate the mass transfer rate of carbon dioxide from a gaseous to a liquid phase. A mass flow controller (Alicat Scientific MC-5SLMP-D) was used to maintain a constant feed. A second mass flow-meter (Alicat Scientific M-5SLMP-D) was used to determine the change in the outlet flow rate. These flowmeters were calibrated by the supplier. Flow Vision SC software supplied by Alicat Scientific was employed to obtain the information about the inlet and outlet flow rates during the absorption experiments. The bubble column reactor works in a batch regime regarding the liquid phase, but in a steady state in relation to the gaseous phase [27].

2.5. Corrosion Experiments

AISI 420 stainless steel was used to prepare the corrosion test specimens. The chemical composition in percentage of the steel was determined by CHNS–O elemental analysis and inductively coupled plasm-mass spectrometry (ICP-MS): Fe-11.51% Cr; 0.712% Mn; 0.324% Ni; 0.1718% C; 0.1121% Cu; 0.1% Si; 0.064% V; 0.027% Co; 0.0261% Mo; 0.0204% N; 0.0122% S; 0.0055% Ca; 0.0017% H; 0.001% Al; 0.0008% K; 0.0005% Zn; 0.0002% Ti; 0.0001% Mg.

The experiments for determining the corrosion behavior of the stainless steel samples were carried out using a potentiostat (Voltalab 21, PGP201 & VoltaMaster 4, Radiometer Analytical) and a three-electrode cell. The accuracy of potential and current readings by the potentiostat is about 0.2%. The electrodes used for the experiments were: the working electrode WE (sample) made of AISI 420, a calomel reference electrode (RE) (XR110, Radiometer Analytical), and an auxiliary electrode of platinum (AE) (Radiometer Analytical, EAC). The samples were cylindrical in shape (diameter = 11.95 mm,

length = 14.90 mm). A solution volume of 400 mL was used for each experiment and a CO_2 (SEO, N-38, 99.98 %) flow of 0.5 L·min^{-1} was introduced into the corrosion cell. The measurements were carried out within the interval of 303.15-323.15 K. A schematic diagram and a more detailed description of the system used for these experiments were reported previously [25].

Before starting the corrosion measurement, an N_2 stream was passed through the cell for 1 h to eliminate the dissolved oxygen in the solution. Then, a carbon dioxide flow is introduced for 1 h to obtain a solution saturated in CO_2. The stream of CO_2 continued throughout the experiment. Then, the potential of the WE versus the RE was measured and recorded until it reached a constant value. Once the system was in equilibrium, the corrosion experiment started, varying the potential applied to the system and recording the current density value for each voltage. The measurements were carried out by applying a potential between −1000 mV and 1000 mV (vs. SCE) with a scan rate of 0.17·mV·s^{-1}. Each experiment was replicated to ensure its reproducibility.

The polarization curves were analyzed according to ASTM standards G1-03 (2017) [28] and G5-14e1 [29]. Tafel extrapolation and the Faraday equation were used to determine both the corrosion density current, i_{corr} (μA·cm^{-2}) and the corrosion rate, *CR* (mm·year^{-1}), for each system:

$$CR = \frac{i_{corr} StM}{nF\rho} \quad (4)$$

where t is the time for which the mass loss is calculated (years), S is the sample surface exposed to the corrosive ambient (cm^2), M is the material molecular mass (g·mol^{-1}), F is the Faraday constant (96,500·C·mol^{-1}), n is the number of electrons lost in the corrosion process, and ρ is the material density (kg·L^{-1}).

In order to investigate the susceptibility to pitting corrosion of AISI 420 subjected to the studied corrosive environments, experiments based on conducting cyclic potentiodynamic polarization were carried out, according to the ASTM standard G-61-86 (2018) [30].

2.6. Solvent Regeneration Studies

For the regeneration studies, based on the stripping procedure, heat was supplied to the solvent rich in carbon dioxide using a heating Selecta Fibroman mantle and a device with a temperature sensor (Selecta Sensoterm). The temperature was monitored during the experimental procedure and two condensers were used to prevent evaporation of the solvent. In order to reduce the decrease in amine concentration, the optimized regeneration time was minimized [31].

3. Results

3.1. Absorption Experiments

MIPA is a primary alkanolamine and, in its reaction with carbon dioxide, has similar behavior to MEA [32,33]. Camacho et al., 1997 [34], indicated that the carbonation relationship (η moles of carbon dioxide·moles of amine^{-1}) in the experiments carried out with MIPA aqueous solutions within the range 0.1–2.0 kmol·m^{-3}, was less than 0.5, which, in agreement with Astarita et al. (1964) [32], indicates that the carbamate was the product of the reaction, and the mechanism would be analogous to that described by Danckwerts, 1979 [35]:

$$RNH_2 + CO_2 \rightleftarrows RNH_2COO^- \text{ (zwitterion)} \quad (5)$$

$$RNH_2 + NH_2COO^- \rightleftarrows R - NH_3^+ + RNHCOO^- \quad (6)$$

Only when $\eta > 0.5$ and alkanolamine concentration is minor than 0.05 kmol·m^{-3}, in addition to Equations (5) and (6), the following reaction would occur:

$$RNHCOO^- + CO_2 + 2H_2O \rightarrow R - NH_3^+ + 2HCO_3^- \quad (7)$$

In the CO_2 absorption by AMP solutions, the carbamate formation is inhibited in the reaction between AMP and CO_2. This is due to AMP, where its sterically hindered structure and its basic behavior are enough small to guarantee that the carbonate ion is always displaced to the bicarbonate formation. In this case, the mean reaction is [36]:

$$RNH_2 + CO_2 + H_2O \rightleftarrows RNH_3^+ + HCO_3^- \quad (8)$$

The dissociation of protonated alkanolamine ion and the carbonate ion formation [37],

$$RNH_3^+ \rightleftarrows RNH_2 + H^+ \quad (9)$$

$$HCO_3^- \rightleftarrows CO_3^{2-} + H^+ \quad (10)$$

Table 1 shows the values of absorbed CO_2 per surface unit of AMP [18], MIPA [34], and AMP+MIPA mixtures for the different temperatures and MIPA concentrations.

Table 1. Flow density of the AMP+MIPA mixtures, AMP [18] and MIPA [34].

AMP Concentration ($kmol \cdot m^{-3}$)	MIPA Concentration ($kmol \cdot m^{-3}$)	$N_A \cdot 10^6$ ($kmol \cdot m^{-2} \cdot s^{-1}$) T (K) = 303.15	$N_A \cdot 10^6$ ($kmol \cdot m^{-2} \cdot s^{-1}$) T (K) = 313.15	$N_A \cdot 10^6$ ($kmol \cdot m^{-2} \cdot s^{-1}$) T (K) = 323.15
1.0	0.00	3.876	6.859	7.36
	0.10	5.147	7.815	8.769
	0.25	5.193	7.945	8.792
	0.50	4.204	5.868	6.962
0.0	0.10	1.010	2.954	4.532
	0.25	1.878	3.430	4.860
	0.50	3.197	4.222	5.325

An increase of the carbon dioxide absorption with the amine mixture is observed, compared to the absorption only by AMP [18] and MIPA [34]. Moreover, the absorption increase is bigger for higher MIPA concentrations up to 0.25 $kmol \cdot m^{-3}$, then, a decrease is observed. These results are similar to those obtained for other mixtures of primary with sterically hindered alkanolamines [15]. The increase in the MIPA concentration causes a higher value of the total amine concentration in the solution and therefore in the carbon dioxide reaction velocity. On the other hand, after reaching a maximum (MIPA = 0.25 $kmol \cdot m^{-3}$), a significant decrease in the reaction velocity is observed. This can be attributed to the influence of the viscosity of the aqueous solution (Table 2), as the presence of MIPA makes this physical property increase considerably [38]. This has a negative effect on the mass transfer velocity.

Therefore, the increase observed for the mixtures of AMP+MIPA cannot be explained using these properties but for an improvement of the hydrodynamic process near the interface. As can be seen in Table 2, the addition of MIPA causes a decrease in the surface tension, inversely proportional to the increase in the carbon dioxide absorption velocity. MIPA aqueous solutions properties have been reported by several authors [38,39].

Concerning the effect of the temperature, it is clearly observed that an increase in the solvent temperature tends to originate positive effects, significantly increasing the carbon dioxide transfer velocity from the gaseous to the liquid phase. This behavior is supported by the fact that the increase in this system parameter causes an increase in the reaction rate and a decrease in the viscosity.

Table 2. Density ρ (g·cm^{-3}), viscosity η (mPa·s), speed of sound c (m·s^{-1}) and surface tension σ (mN·m^{-1}) of AMP+MIPA from T (K) = 303.15 to 323.15 K.

AMP Concentration (kmol·m^{-3})	MIPA Concentration (kmol·m^{-3})	T (K) = 303.15	T (K) = 313.15	T (K) = 323.15
		ρ (g·cm^{-3})	ρ (g·cm^{-3})	ρ (g·cm^{-3})
1.0	0.00	0.994111	0.98869	0.981359
	0.10	0.994254	0.989225	0.98231
	0.25	0.994411	0.989863	0.982751
	0.50	0.994661	0.990185	0.983855
		η (mPa·s)	η (mPa·s)	η (mPa·s)
1.0	0.00	1.08935270	0.81854676	0.62634402
	0.10	1.13021224	0.85803828	0.65123491
	0.25	1.18065910	0.89676943	0.68355647
	0.50	1.26791521	0.96210583	0.73541749
		c (m·s^{-1})	c (m·s^{-1})	c (m·s^{-1})
1.0	0.00	1572.66	1583.08	1588.03
	0.10	1576.92	1587.00	1591.90
	0.25	1583.23	1591.57	1596.12
	0.50	1594.65	1601.33	1603.34
		σ (mN·m^{-1})	σ (mN·m^{-1})	σ (mN·m^{-1})
1.0	0.00	52.11	43.92	40.09
	0.10	47.19	41.00	39.00
	0.25	45.48	39.81	39.12
	0.50	47.28	44.18	43.29

3.2. Corrosion Studies

Alkanolamines are not corrosive substances [9,40], but there is an increase in the corrosion rate when they absorb carbon dioxide.

There are several iron corrosion mechanisms in aqueous solutions in presence of CO_2, even if the amount of this compound is low. An example is the one proposed by Davies et al. (1980) [41], where the iron disintegration occurs in a bicarbonate solution, according to the reactions, shown in Equations (11)–(14):

$$Fe + 2H_2O \rightarrow Fe(OH)_2 + 2H^+ + 2e^- \quad (11)$$

$$Fe + HCO_3^- \rightarrow FeCO_3 + H^+ + 2e^- \quad (12)$$

$$Fe + HCO_3^- \rightarrow FeCO_3 + H^+ + 2e^- \quad (13)$$

$$FeCO_3 + HCO_3^- \rightarrow Fe(CO_3)_2^{2-} + H^+ \quad (14)$$

On the other hand, the dissolved oxygen can increase the system corrosiveness [42], oxidizing the metallic surface originating an oxide layer according to the reactions shown in Equations (15) and (16):

$$2Fe + 2H_2O + O_2 \rightarrow 2Fe(OH)_2 \quad (15)$$

$$2Fe(OH)_2 + 2H_2O + \frac{1}{2}O_2 \rightarrow 2Fe(OH)_3 \quad (16)$$

Due to the corrosion problems originated by the use of alkanolamines, corrosion experiments were performed and the polarization curves were plotted for the different alkanolamine mixtures in order to study the influence of the temperature and the composition of the solution on the corrosion rate. The electrochemical parameters and the corrosion rate (Table 3) were obtained for AISI 420 steel in AMP+MIPA aqueous solutions by means of the Tafel method [43].

Table 3. AISI 420 electrochemical parameters of aqueous AMP+MIPA solutions in presence of CO_2.

AMP Concentration (kmol·m^{-3})	MIPA Concentration (kmol·m^{-3})	T (K)	E_{corr} (mV)	β_a (mV·Decade^{-1})	β_c (mV·Decade^{-1})	i_{corr} (μA·cm^{-2})	CR (mm·Year^{-1})
1.0	0.10	303	−391.65	150.66	−161.25	2.783	0.216
		313	−691.83	171.97	−72.80	4.313	0.335
		323	−713.90	162.02	−81.39	7.523	0.584
	0.25	303	−700.70	211.44	−87.97	1.185	0.092
		313	−605.21	173.22	−180.66	1.469	0.114
		323	−599.02	113.98	−153.02	2.963	0.230
	0.50	303	−447.20	151.81	−155.00	0.464	0.036
		313	−696.27	215.03	−53.64	0.609	0.047
		323	−737.20	64.58	−43.37	2.053	0.159

The influence of the solution temperature is observed in the Tafel curves shown in Figure 1. In this figure, we observe a displacement of the curves to the right with the increase in the temperature, which implies a higher value of current density. The effect of the temperature on the corrosion rate is shown in Figure 2.

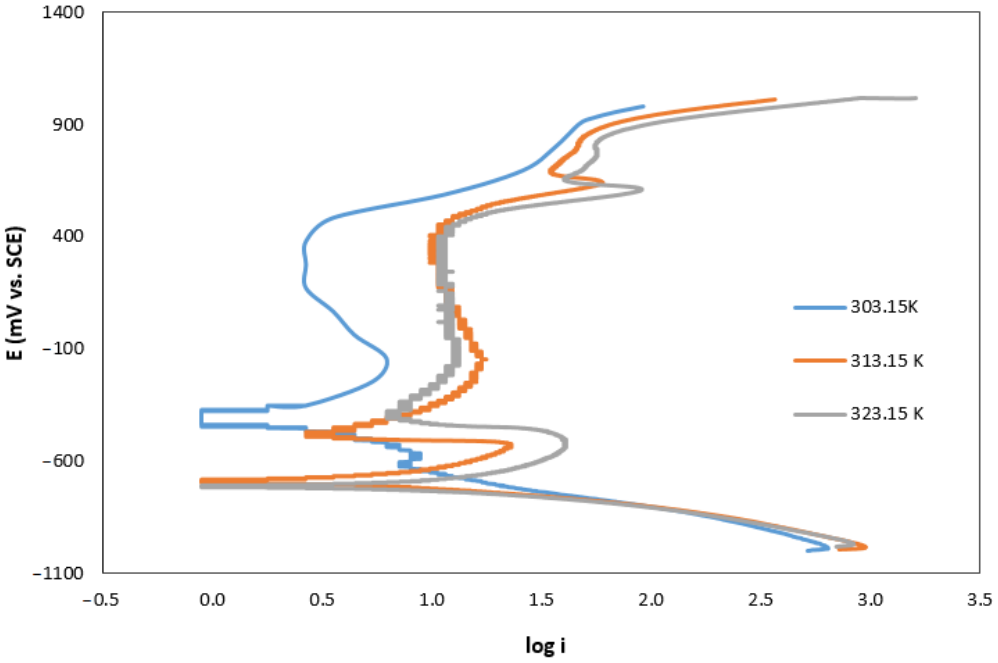

Figure 1. Temperature effect on Tafel curves of AISI 420 in AMP+MIPA (1:0.10) solutions.

It is known that the temperature is an important parameter for the reaction kinetics, producing an increase in its speed. In the CO_2 absorption by AMP and MIPA, the reactions shown in Equations (5) and (8) are accelerated by the increase in the temperature, originating an increase of RNH_3^+ and HCO_3^-. The increase of these products makes reactions change to keep the balance and, therefore, higher amounts of H^+ are generated in the system.

The metal dissolution reaction, shown in Equation (17), is an anodic reaction of the electrochemical process, while the oxidizer reduction reaction, shown in Equation (18), is cathodic.

$$Fe \rightarrow Fe^{2+} + 2e^- \quad (17)$$

$$2H^+ + 2e^- \rightarrow H_2 \quad (18)$$

When the amount of H^+ increases with the temperature, the balance between the reactions, shown in Equations (17) and (18), is broken. To keep the equilibrium, more metal

is dissolved, originating a higher electron generation for the oxidizer reduction. In response to the balance breakdown, the effect of the increase in the temperature is to speed up the reactions, shown in Equations (17) and (18), and, therefore, increase the corrosion rate.

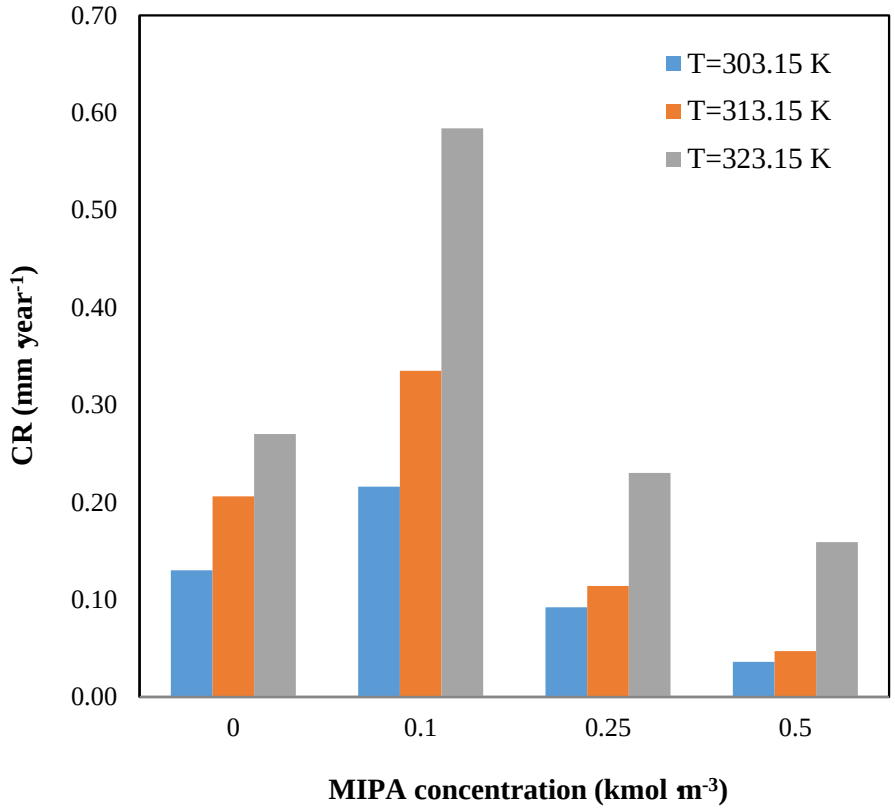

Figure 2. Effect of the temperature and composition on the corrosion rate.

3.3. Effect of the Absorbent Composition on Corrosion Rate

Figure 2 shows the influence of the solution composition on the corrosion rate. An increase in the MIPA concentration causes an increase in the corrosion rate, reaching a maximum for a MIPA concentration of 0.1 kmol·m^{-3}. For these cases, in the carbon dioxide absorption by MIPA, apart from the reactions shown in Equations (5) and (6), the reaction shown in Equation (7) takes place, as the carbonation relationship is >0.5 [34], so the amount of bicarbonate in the system increases, being this compound the major cause of the steel corrosion.

With increasing MIPA concentration, the carbonation relationship is <0.5, and the reaction, shown in Equation (7), does not occur, so the corrosion rate decreases. Moreover, with increasing the total amine concentration in the mixture, the amount of water in the solution decreases, and the number of bicarbonate ions obtained from the carbamate hydrolysis is also lower, so added to the higher solution viscosity (Table 2) which makes the diffusion difficult and produces a decrease in the corrosion rate.

In addition, these mixtures present a lower corrosiveness than the solutions with only one alkanolamine.

The susceptibility to pitting corrosion was investigated using the cyclic potentiodynamic polarization technique (Figure 3). Since the reverse curve is on the left of the forward curve, it was not likely to have pitting corrosion in the system.

From the results of the corrosion studies, the blend of AMP (1 kmol·m^{-3}) and MIPA (0.25 kmol·m^{-3}) is less corrosive.

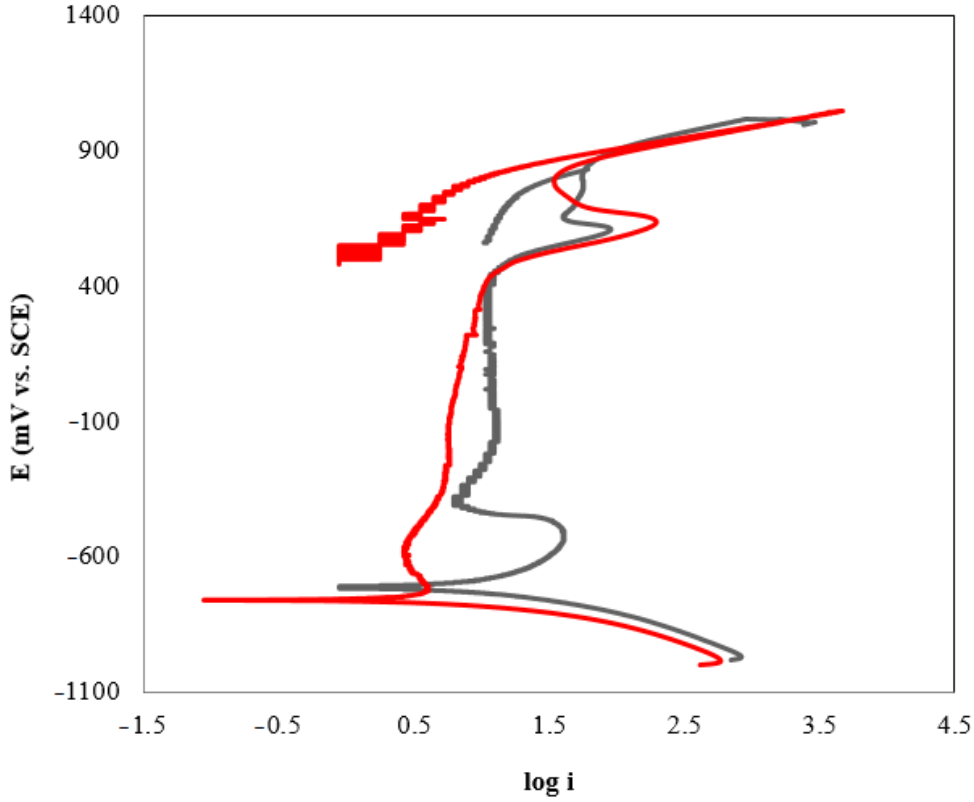

Figure 3. Cyclic polarization curves of AISI 420 in AMP+MIPA+CO_2 systems: (−) AMP+MIPA (1:0.1); (−) AMP+MIPA (1:0.5).

3.4. Bubble Column Studies

Once the studies related to the carbon dioxide absorption and the corrosion behavior of the MIPA and AMP blends were carried out, it becomes interesting to carry out additional studies using the ratio of the mixture of amines with better results. Specifically, the total amine concentration of 1.25 kmol·m^{-3} (1 kmol·m^{-3} for AMP and 0.25 kmol·m^{-3} for MIPA), has been used in other types of contact equipment, such as a bubble column.

An example of the studies in relation to the carbon dioxide absorption curves using individual amines and blend is shown in Figure 4. It can be clearly seen that the shape of the absorption curves of the different solvents show quite different behaviors.

When only AMP in the solvent is used, a practically linear decrease is observed as the amine present in the liquid phase is consumed. This behavior is very different from that shown in the experiments in which only MIPA was used in the solvent. In the latter case, a decrease in the absorption rate is observed after 1000 s of the experiment had elapsed. The solvent based on MIPA does not reach carbon dioxide absorption rates higher than those shown by the solvent based only on AMP.

This different behavior is due to the characteristics of the molecules used to carry out the chemical absorption of carbon dioxide. Specifically, in the case of AMP there is a significant degree of steric hindrance [6] that makes the chemical reaction process have a different mechanism.

For non-sterically hindered amines, and specifically in the case of the use of aqueous solutions of MIPA, the main reaction that occurs during the chemical absorption of carbon dioxide is that carbamate is generated as a reaction product [34]. That reaction mechanism causes two amine molecules to be consumed for each molecule of carbon dioxide, as previously indicated in reactions shown in Equations (5) and (6). This fact causes the amine to be consumed very quickly and therefore a decrease of the reaction rate and therefore the rate of absorption of carbon dioxide occurs. When AMP is used in the solvent, the

behavior of the absorption curve does not show a drop in the absorption rate. As in the case of MIPA, the initial reaction is the formation of carbamate, but due to the high degree of steric hindrance, hydrolysis of this compound occurs forming bicarbonate [34]. This reaction mechanism causes the global stoichiometry to be one mole of amine per mole of carbon dioxide. This behavior helps to maintain a higher reaction rate, as the data from the absorption curves reveal.

Finally, Figure 4 also shows the comparison between the absorption curves of the individual amines and the corresponding to the mixture of amines that have previously shown better results related to corrosion processes. The behavior shown by the mixture of amines is very similar to that previously described for the solvent based on AMP. Only a slight decrease in absorption rate was observed due to the presence of MIPA. The use of the mixture of amines maintains the absorption rate in times greater than 2000 s. It should be taken into account that in the industrial absorbers during the carbon dioxide absorption stage, only a carbon dioxide charge between 0.4–0.6 mol of CO_2 per mol of amine is reached.

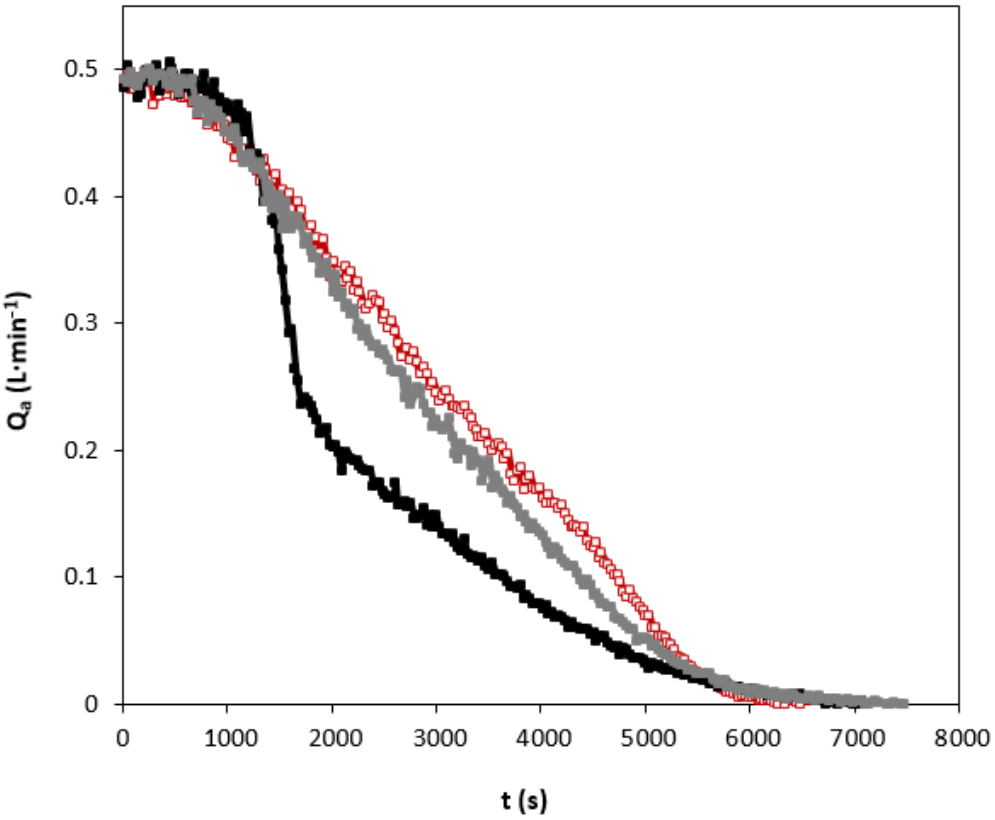

Figure 4. Carbon dioxide absorption curves using individual amines and blend. Q_G = 0.5 L·min^{-1}. Total amines concentration of 1.25 kmol·m^{-3}. (□) AMP; (■) MIPA; (■) AMP+MIPA (1:0.25).

Taking into account the importance of the carbon dioxide charge that can be achieved in the chemical solvent, Figure 5 shows the behavior of this parameter for the different solvents analyzed in this section. The results are consistent with the conclusions previously reached by analyzing the carbon dioxide absorption curves. Due to the behavior shown by the solvent based on MIPA, the area under the curve that is related to the carbon dioxide charge is smaller than in the case of the other chemical solvents (AMP and AMP+MIPA). The behavior is promising because the absorption drop with respect to fresh solvent is relatively low in comparison with other commonly used solvents [11], but the most important thing is that the degree of regeneration is subsequently maintained. When the amines mixture for the separation of carbon dioxide is used, a decrease is also observed in comparison with the use of AMP only. However, the most relevant aspect is that the

rate at which carbon dioxide is captured is the same for both solvents during most of the experiment.

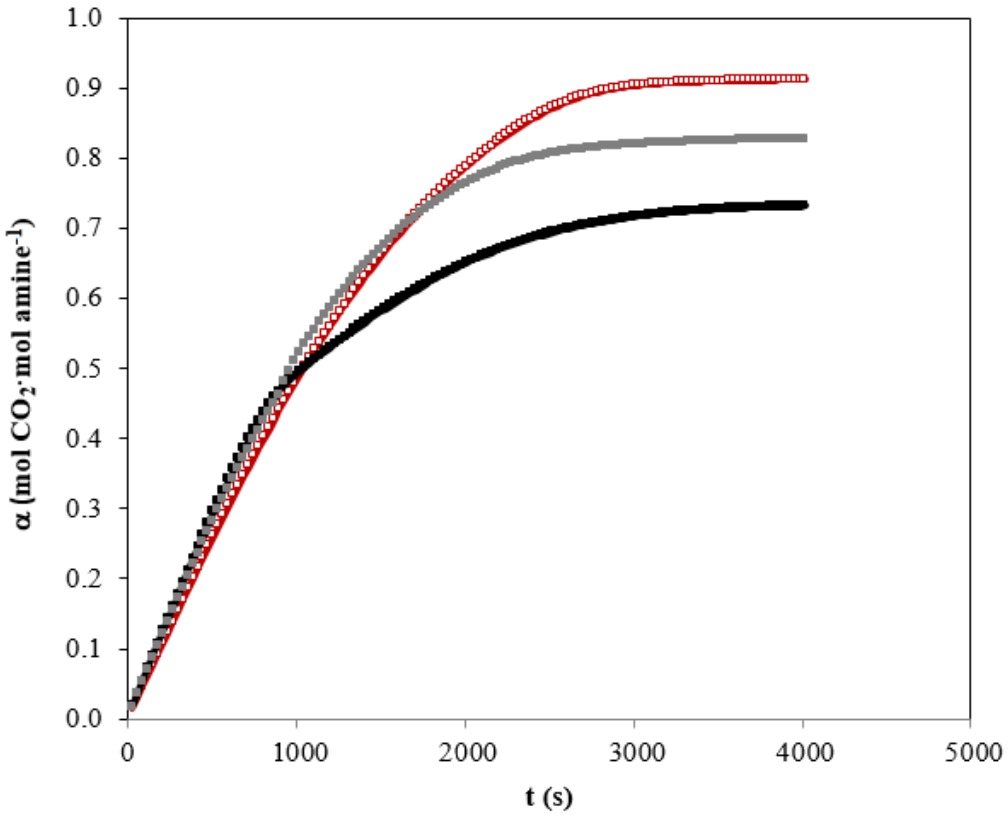

Figure 5. Carbon dioxide loading using individual amines and blend. Q_G = 0.5 L·min^{-1}. Total amines concentration of 1.25 kmol·m^{-3}. (□) AMP; (■) MIPA; (■) AMP+MIPA (1:0.25).

3.5. Solvent Regeneration Studies

When a chemical solvent is being evaluated for carbon dioxide separation we must evaluate the regeneration capacity. It should be taken into account that during the regeneration process, solvent degradation processes can also occur. The experimental data of the solvent carbon dioxide absorption curve based on the mixture of fresh AMP and MIPA (1:0.25) and after different cycles of absorption and regeneration are shown in Figure 6. A fall in the capture capacity of carbon dioxide is observed after the first regeneration (around 15%), although different absorption/regeneration cycles are carried out where no further decreases occur.

This behavior is typically observed [44] since during the first regeneration all the reaction products cannot be returned to reagents due to the equilibrium counter of the protonated amine/amine process.

The behavior is promising because the absorption drop with respect to fresh solvent is relatively low, but the most important thing is that the degree of regeneration is subsequently maintained.

Figure 7 shows a comparison between the individual amines behavior and the blend. A similar decrease to that observed for the use of AMP is observed, while the use of MIPA shows a very important decrease. In addition, in the case of the use of MIPA, the carbon dioxide load is lower than for AMP or AMP+MIPA (Figure 6) so the behavior is even worse.

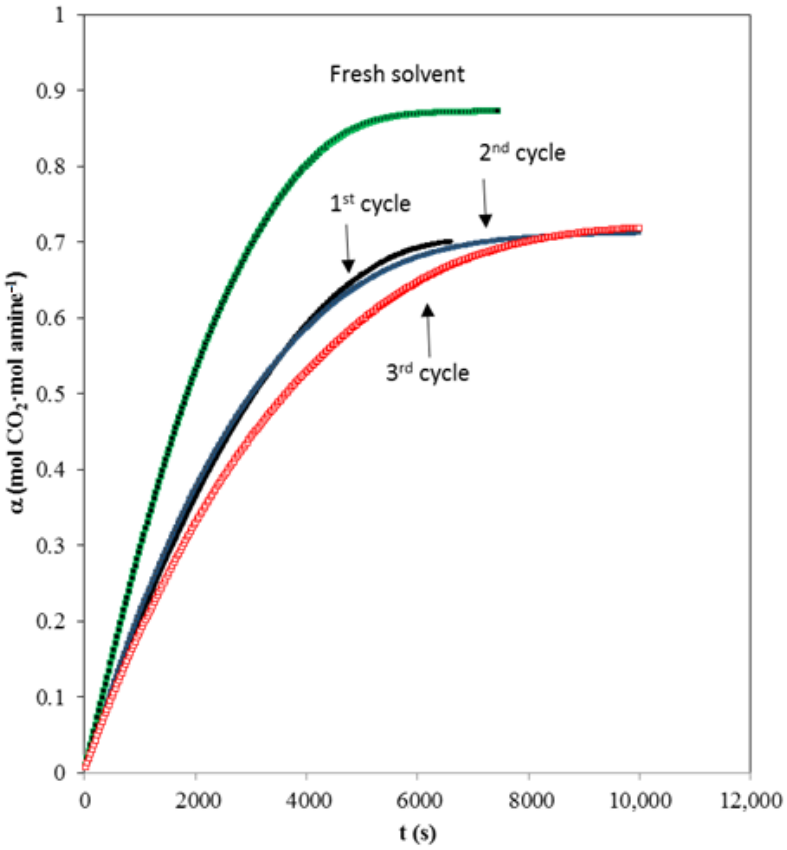

Figure 6. Influence of regeneration cycle upon absorption curve Q = 0.5 L·min^{-1}. Total amine concentration of 1.25 kmol·m^{-3}. (■) fresh solvent, (■) 1st cycle; (□) 2nd cycle, (□) 3rd cycle.

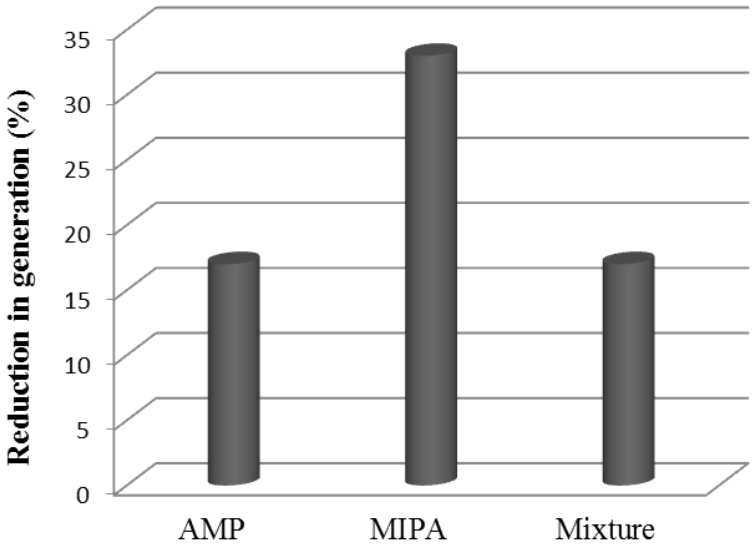

Figure 7. Reduction of the degree of regeneration with respect to the fresh solvent. Mixture = AMP+MIPA (1:0.25).

4. Conclusions

AMP+MIPA aqueous solutions have been analyzed during the carbon dioxide absorption process considering its corrosivity. The carbon dioxide absorption of the mixtures is higher compared to individual AMP or MIPA. An improvement of the hydrodynamic

process in the vicinity of the interface caused by a decrease in the surface tension occurs, inversely proportional to the increase in the carbon dioxide absorption velocity. The increment of the total amine concentration initially, the lower chemical reaction velocity of MIPA, and its high viscosity justify the behavior. The corrosivity of the mixtures increases with MIPA concentration, reaching a maximum and then decrease. This behavior could be explained by the carbonation relationship values during the carbon dioxide absorption. In this kind of system, no pitting corrosion has been observed.

Of the mixtures studied, the blend of AMP (1 kmol·m^{-3}) and MIPA (0.25 kmol·m^{-3}) which has high CO_2 absorption and less corrosive, is studied deeply. It has also shown good results regarding regeneration degree, absorption rate, and carbon dioxide loading in the bubble column reactor with similar results to an AMP-solvent.

Author Contributions: Conceptualization and investigation, M.D.L.R. and D.G.-D.; methodology, investigation and formal analysis, A.S.-B., A.J.M., and E.M.P.; writing—review and editing, M.D.L.R. and D.G.-D. All authors have read and agreed to the final manuscript before submission.

Funding: Financial support for this research was obtained under the Project UJA 2016/08/07: "Development of more efficient solvents for carbon dioxide capture-2" (I+D+i Support Plan of the University of Jaen), for which we are grateful.

Institutional Review Board Statement: Not applicable.

Informed Consent Statement: Not applicable.

Data Availability Statement: Data is contained within the article.

Conflicts of Interest: The authors declare no conflict of interest.

Abbreviations

Symbols used

A	[m^2]	Reactor area
c	[m·s^{-1}]	Speed of sound
C_{BO}	[kmol·m^{-3}]	Concentration
CR	[mm·year^{-1}]	Corrosion rate
E_{corr}	[mV]	Electrochemical potential
F	[C ·mol^{-1}]	Faraday constant
i_{corr}	[μA·cm^{-2}]	Corrosion density
M	[g·mol^{-1}]	Material molecular mass
n		Number of electrons
N_A	[kmol·m^{-2}·s^{-1}]	Flow density
P	[kPa]	Total pressure
Q'	[m^3 ·s^{-1}]	Volumetric gas flow rate
R	[kPa· m^3 ·K^{-1}·kmol^{-1}]	Gas constant
S	[cm^2]	Surface exposed to the corrosive ambient
T	[K]	Temperature
t	[s]	Time

Greek symbols

α	[moles of carbon dioxide·moles of amine^{-1}]	CO_2 loading
η	[moles of carbon dioxide·moles of amine^{-1}]	Carbonation relationship
ρ	[g·cm^{-3}]	Density
η	[mPa·s]	Viscosity
σ	[mN·m^{-1}]	Surface tension
β_a	[mV·decade^{-1}]	Anodic slope
β_C	[mV·decade^{-1}]	Cathodic slope
K	[-]	Constant of the used capillaries
θ	[-]	Correction value

References

1. Paraschiv, S.; Paraschiv, L.S. Trends of carbon dioxide (CO_2) emissions from fossil fuels combustion (coal, gas and oil) in the EU member states from 1960 to 2018. *Energy Rep.* **2020**, *6*, 237–242. [CrossRef]
2. Mardani, A.; Streimikiene, D.; Cavallaro, F.; Loganathan, N.; Khoshnoudi, M. Carbon dioxide (CO_2) emissions and economic growth: A systematic review of two decades of research from 1995 to 2017. *Sci. Total. Environ.* **2019**, *649*, 31–49. [CrossRef] [PubMed]
3. Sovacool, B.K.; Griffiths, S.; Kim, J.; Bazilian, M. Climate change and industrial F-gases: A critical and systematic review of developments, sociotechnical systems and policy options for reducing synthetic greenhouse gas emissions. *Renew. Sustain. Energy Rev.* **2021**, *141*, 110759. [CrossRef]
4. Mandald, B.; Bandyopadhyay, S.S. Simultaneous Absorption of CO_2 and H_2S Into Aqueous Blends ofN-Methyldiethanolamine and Diethanolamine. *Environ. Sci. Technol.* **2006**, *40*, 6076–6084. [CrossRef] [PubMed]
5. Faiz, R.; Al-Marzouqi, M. Mathematical modeling for the simultaneous absorption of CO_2 and H_2S using MEA in hollow fiber membrane contactors. *J. Membr. Sci.* **2009**, *342*, 269–278. [CrossRef]
6. Soosaiprakasam, I.R.; Veawab, A. Corrosion and polarization behavior of carbon steel in MEA-based CO_2 capture process. *Int. J. Greenh. Gas Control.* **2008**, *2*, 553–562. [CrossRef]
7. Kittel, J.; Fleury, E.; Vuillemin, B.; Gonzalez, S.; Ropital, F.; Oltra, R. Corrosion in alkanolamine used for acid gas removal: From natural gas processing to CO_2 capture. *Mater. Corros.* **2010**, *63*, 223–230. [CrossRef]
8. Sema, T.; Naami, A.; Fu, K.; Edali, M.; Liu, H.; Shi, H.; Liang, Z.; Idem, R.; Tontiwachwuthikul, P. Comprehensive mass transfer and reaction kinetics studies of CO_2 absorption into aqueous solutions of blended MDEA-MEA. *Chem. Eng. J.* **2012**, *209*, 501–512. [CrossRef]
9. DuPart, M.S.; Bacon, T.R.; Edwards, D.J. Understanding corrosion in alkanolamine gas treating plants. 1. Proper mechanism diagnosis optimizes amine operations. *Hydrocarb. Process* **1993**, *72*, 75–80.
10. Kittel, J.; Gonzalez, S. Corrosion in CO_2 post-combustion capture with alkanolamines. A review. *Oil Gas Sci. Technol. Revue IFP Energies Nouv.* **2014**, *69*, 915–929. [CrossRef]
11. Schäffer, A.; Brechtel, K.; Scheffknecht, G. Comparative study on differently concentrated aqueous solutions of MEA and TETA for CO_2 capture from flue gases. *Fuel* **2012**, *101*, 148–153. [CrossRef]
12. Saha, A.K.; Bandyopadhyay, S.S.; Biswas, A.K. Kinetics of absorption of CO_2 into aqueous solutions of 2-amino-2-methyl-1-propanol. *Chem. Eng. Sci.* **1995**, *50*, 3587–3598. [CrossRef]
13. Patil, M.P.; Vaidya, P.D. Characterization of the superior CO_2-capturing absorbent blend AMP/PZ/EGMEE/Water. *Int. J. Greenh. Gas Control.* **2019**, *84*, 29–35. [CrossRef]
14. Nwaoha, C.; Tontiwachwuthikul, P.; Benamor, A. CO_2 capture from lime kiln using AMP-DA2MP amine solvent blend: A pilot plant study. *J. Environ. Chem. Eng.* **2018**, *6*, 7102–7110. [CrossRef]
15. Shi, H.; Cui, M.; Fu, J.; Dai, W.; Huang, M.; Han, J.; Quan, L.; Tontiwachwuthikul, P.; Liang, Z. Application of "coordinative effect" into tri-solvent MEA+BEA+AMP blends at concentrations of 0.1 + 2 + 2~0.5 + 2 + 2 mol/L with absorption, desorption and mass transfer analyses. *Int. J. Greenh. Gas Control.* **2021**, *107*, 103267. [CrossRef]
16. Barbarossa, V.; Barzagli, F.; Mani, F.; Lai, S.; Stoppioni, P.; Vanga, G. Efficient CO_2 capture by non-aqueous 2-amino-2-methyl-1-propanol (AMP) and low temperature solvent regeneration. *RSC Adv.* **2013**, *3*, 12349–12355. [CrossRef]
17. Qian, Z.; Xu, L.-B.; Li, Z.-H.; Li, H.; Guo, K. Selective Absorption of H_2S from a Gas Mixture with $CO_2$by AqueousN-Methyldiethanolamine in a Rotating Packed Bed. *Ind. Eng. Chem. Res.* **2010**, *49*, 6196–6203. [CrossRef]
18. Camacho, F.; Sanchez, S.; Pacheco, R.; Sanchez, A.; La Rubia, M.D. Thermal effects of CO_2 absorption in aqueous solutions of 2-amino-2-methyl-1-propanol. *AIChE J.* **2005**, *51*, 2769–2777. [CrossRef]
19. Dubois, L.; Mbasha, P.K.; Thomas, D. CO_2 Absorption into Aqueous Solutions of a Polyamine (PZEA), a Sterically Hindered Amine (AMP), and their Blends. *Chem. Eng. Technol.* **2010**, *33*, 461–467. [CrossRef]
20. Bougie, F.; Iliuta, M.C. Sterically Hindered Amine-Based Absorbents for the Removal of CO_2 from Gas Streams. *J. Chem. Eng. Data* **2012**, *57*, 635–669. [CrossRef]
21. Veawab, A.; Tontiwachwuthikul, P.; Bhole, S.D. Studies of Corrosion and Corrosion Control in a CO_2−2-Amino-2-methyl-1-propanol (AMP) Environment. *Ind. Eng. Chem. Res.* **1997**, *36*, 264–269. [CrossRef]
22. Veawab, A.; Tontiwachwuthikul, P.; Chakma, A. Influence of Process Parameters on Corrosion Behavior in a Sterically Hindered Amine−CO_2 System. *Ind. Eng. Chem. Res.* **1999**, *38*, 310–315. [CrossRef]
23. Veawab, A.; Tontiwachwuthikul, P.; Chakma, A. Corrosion Behavior of Carbon Steel in the CO_2 Absorption Process Using Aqueous Amine Solutions. *Ind. Eng. Chem. Res.* **1999**, *38*, 3917–3924. [CrossRef]
24. Tanthapanichakoon, W.; Veawab, A.; McGarvey, B. Electrochemical Investigation on the Effect of Heat-stable Salts on Corrosion in CO_2 Capture Plants Using Aqueous Solution of MEA. *Ind. Eng. Chem. Res.* **2006**, *45*, 2586–2593. [CrossRef]
25. Palmero, E.M.; La Rubia, M.D.; Sánchez-Bautista, A.; Pacheco, R.; Sanchez, S. Study of corrosion of AISI 420 in the CO_2 absorption process using 2-amino-2-methyl-1-propanol aqueous solutions. *Corros. Eng. Sci. Technol.* **2013**, *48*, 136–142. [CrossRef]
26. Camacho, F.; Sánchez, S.; Pacheco, R.; La Rubia, M.D.; Sánchez, A. Kinetics of the reaction of pure CO_2 with N -methyldiethanolamine in aqueous solutions. *Int. J. Chem. Kinet.* **2008**, *41*, 204–214. [CrossRef]
27. López, A.B.; Gómez-Díaz, D.; La Rubia, M.D.; Navaza, J.M. Effect of Carbon Dioxide Chemical Absorption on Bubble Diameter and Interfacial Area. *Chem. Eng. Technol.* **2013**, *36*, 1968–1974. [CrossRef]

28. ASTM G1-03 (2017) e1. *Standard Practice for Preparing, Cleaning, and Evaluating Corrosion Test Specimens*; ASTM International: West Conshohocken, PA, USA, 2017.
29. ASTM G5-14e1. *Standard Reference Test Method for Making Potentiodynamic Anodic Polarization Measurements*; ASTM International: West Conshohocken, PA, USA, 2014.
30. ASTM G61-86. *Standard Test Method for Conducting Cyclic Potentiodynamic Polarization Measurements for Localized Corrosion Susceptibility of Iron-, Nickel-, or Cobalt-Based Alloys*; ASTM International: West Conshohocken, PA, USA, 2018.
31. Baltar, A.; Gómez-Díaz, D.; Navaza, J.M.; Rumbo, A. Absorption and regeneration studies of chemical solvents based on dimethylethanolamine and diethylethanolamine for carbon dioxide capture. *AIChE J.* **2020**, *66*, 1. [CrossRef]
32. Astarita, G.; Marrucci, G.; Gioia, F. The influence of carbonation ratio and total amine concentration on carbon dioxide absorption in aqueous monoethanolamine solutions. *Chem. Eng. Sci.* **1964**, *19*, 95–103. [CrossRef]
33. Blauwhoff, P.; Versteeg, G.; Van Swaaij, W. A study on the reaction between CO_2 and alkanolamines in aqueous solutions. *Chem. Eng. Sci.* **1984**, *39*, 207–225. [CrossRef]
34. Camacho, F.; Sanchez, S.; Pacheco, R. Absorption of Carbon Dioxide at High Partial Pressures in 1-Amino-2-propanol Aqueous Solution. Considerations of Thermal Effects. *Ind. Eng. Chem. Res.* **1997**, *36*, 4358–4364. [CrossRef]
35. Danckwerts, P. The reaction of CO_2 with ethanolamines. *Chem. Eng. Sci.* **1979**, *34*, 443–446. [CrossRef]
36. Chakraborty, A.; Astarita, G.; Bischoff, K. CO_2 absorption in aqueous solutions of hindered amines. *Chem. Eng. Sci.* **1986**, *41*, 997–1003. [CrossRef]
37. Danckwerts, P.; McNeil, K. The absorption of carbon dioxide into aqueous amine solutions and the effects of catalysis. *Insights Into Chem. Eng.* **1981**, *45*, T32–T49. [CrossRef]
38. Rayer, A.V.; Kadiwala, S.; Narayanaswamy, K.; Henni, A. Volumetric Properties, Viscosities, and Refractive Indices for Aqueous 1-Amino-2-Propanol (Monoisopropanolamine (MIPA)) Solutions from (298.15 to 343.15) K. *J. Chem. Eng. Data* **2010**, *55*, 5562–5568. [CrossRef]
39. Alvarez, E.; Cancela, Á.; Maceiras, R.; Navaza, J.M.; Táboas, R. Surface Tension of Aqueous Binary Mixtures of 1-Amino-2-Propanol and 3-Amino-1-Propanol, and Aqueous Ternary Mixtures of These Amines with Diethanolamine, Triethanolamine, and 2-Amino-2-methyl-1-propanol from (298.15 to 323.15) K. *J. Chem. Eng. Data* **2003**, *48*, 32–35. [CrossRef]
40. DuPart, M.S.; Bacon, T.R.; Edwards, D.J. Understanding corrosion in alkanolamine gas treating plants. 2. *Hydrocarb. Process* **1993**, *72*, 89–94.
41. Davies, D.H.; Burstein, G.T. The Effects of Bicarbonate on the Corrosion and Passivation of Iron. *Corrosion* **1980**, *36*, 416–422. [CrossRef]
42. Fontana, M.G. *Corrosion Engineering*; McGraw-Hill: New York, NY, USA, 1986.
43. Tafel, J.; Schmitz, K.; Naremann, K.; Emmert, B. Uber die Polarization bei Kathodischer der Protonuebertragung. *Z. Phys. Chem.* **1905**, *50*, 641.
44. Lopez, A.; La Rubia, M.D.; Navaza, J.; Pacheco, R.; Gómez-Díaz, D. Characterization of MIPA and DIPA aqueous solutions in relation to absorption, speciation and degradation. *J. Ind. Eng. Chem.* **2015**, *21*, 428–435. [CrossRef]